Intergranular fracture in model polycrystals with correlated distribution of low-angle grain boundaries

Clinton DeW. Van Siclen*
Idaho National Laboratory, Idaho Falls, Idaho 83415-2211, USA
(Received 16 January 2006; revised manuscript received 9 April 2006; published 18 May 2006)

Grain boundary engineering of materials is intended to increase the fraction of "special" boundaries that possess preferred properties. These may be low-angle boundaries with good mechanical and corrosion resistance properties. In this case, the distribution of special boundaries is spatially correlated rather than random, due to crystallographic constraints. Such a correlated distribution, in addition to the density of special boundaries, will likely affect the progression of damage and failure of a polycrystalline material under load or applied strain. This is demonstrated for a two-dimensional model polycrystal, which is an array of hexagonal grains defining a "honeycomb" network of grain boundary facets. The facets are assigned a high or low elasticity modulus in accordance with their "special" or "nonspecial" designation, respectively. Then damage evolution due to an increasing strain is monitored as the following sequence of two steps is repeated until material failure: (1) calculation of the stress and strain fields by use of a scalar Hooke's law and (2) rupture of the facet with greatest strain energy. For polycrystals with a high fraction of special facets, damage proceeds by a series of "bursts" ("avalanches") of single-facet failures distributed over the polycrystal. These failures occur at special facets that connect two clusters of nonspecial facets, thereby creating larger clusters of "weak" (nonspecial plus ruptured) facets oriented roughly perpendicular to the applied strain. Eventually a weak cluster grows to a critical size such that sufficient stress is diverted through the nonspecial facets (which have served as ligaments preventing a crack from nucleating on the weak cluster) to cause those facets to fail. This crack growth leads to catastrophic failure of the model polycrystal.

DOI: 10.1103/PhysRevB.73.184118 PACS number(s): 62.20.Mk, 61.72.Mm

I. INTRODUCTION

The network of grain boundaries contained in a polycrystal represents a connected defect structure on which microcracks may nucleate and grow in response to a stress or strain applied to the polycrystal. Presumably the ratio of low- to high-angle boundaries will significantly influence the progression of damage. Indeed, this expectation motivates the current interest in "grain boundary engineering" (GBE),[1,2] where the formation of "good" (special) boundaries is promoted [at the expense of "bad" (nonspecial) boundaries] by a series of processing steps.[3] Special boundaries are low-angle or high-coincidence grain boundaries that, by their regular atomic structure, are highly cohesive and have a low solubility for embrittling impurities.[2,4]

Various authors[5–7] have suggested that the spatial distribution, in addition to the number density, of special boundaries should influence the mechanical properties of a polycrystal. For example, clusters of special boundaries are obstacles to crack propagation. Frary and Schuh[6,7] have emphasized that the crystallographic constraint (e.g., in a two-dimensional polycrystal, the misorientation angles around a triple junction sum to 360°) must produce a nonrandom distribution of low-angle (special) boundaries: most notably, a surfeit of special triple junctions and clustering of those triple junctions.

It is thus of interest to consider the effects of such a *correlated* distribution of special boundaries on damage progression and failure. As an initial effort in this direction, a two-dimensional (2D) model of a polycrystal with special and nonspecial grain boundary facets is presented in the following section. This model is a 2D array of identical, hexagonal grains, which gives rise to a honeycomb network of grain boundary facets (for example, three grains produce a boundary triple junction). The facets are identified as special or nonspecial in accordance with the crystallographic constraint and are assigned high and low values, respectively, of the elasticity modulus to effect the local response to the applied stress or strain. For computational convenience, the stress and strain fields are related by a scalar version of Hooke's law. The system evolves (i.e., damage proceeds) as facets fail upon reaching a threshold value of the local strain energy.

Simulations presented in a subsequent section show damage accumulation by a series of "avalanches," or "bursts," of spatially distributed, single-facet failures, where each avalanche is triggered by an increase in the strain applied to the model polycrystal. For polycrystals with a high fraction of special facets, these single-facet failures weaken the material by connecting clusters of nonspecial facets that are oriented roughly perpendicular to the applied field direction. With additional applied strain, a crack nucleates on such a "weak" facet cluster and immediately grows to span the polycrystal. For polycrystals with a low fraction of special facets, the single-facet failures occur at the boundaries of large, irregularly shaped grains. These distinct progressions are consequences of the crystallographic constraint, as it produces clusters of nonspecial facets that are more elongated and fibrous (due to the prevalence of nonspecial double junctions), and clusters of special facets that are more ramified (due to the prevalence of special triple junctions), than result from a random distribution of special and nonspecial facets.

II. POLYCRYSTAL MODEL

The two-dimensional, simulated polycrystal is an array of hexagonal grains oriented such that one-third of all facets are perpendicular to the direction of the applied stress or strain. Facets are either of special or nonspecial type, distinguished by a high or low value, respectively, of the elasticity modulus μ. No other source of heterogeneity (e.g., nonuniform grain size distribution) is considered here.

The spatial correlation of special facets is a consequence of the crystallographic constraint. Consider, for example, an *isotropic* polycrystal, where no restrictions are placed on the possible crystallographic orientations of the grains. Then, given the probability p_s that an arbitrarily selected facet is special, there is a probability p_s^2 that two connecting facets are both special, since adjacent grains have independent crystallographic orientations (this statement is *not* true for *anisotropic* polycrystals, as is shown in Appendix A). But if two facets meeting at a junction are special (so that crystal misalignment across two boundaries is small), the crystallographic constraint ensures that the third has a greater than p_s probability of being special as well. That is, the probability p_3 that an arbitrarily selected triple junction in a correlated polycrystal connects *three* special facets is greater than p_s^3, which is the case for a random polycrystal.

To assign special or nonspecial status to the facets of a correlated polycrystal, each hexagonal grain is assigned a crystal orientation angle θ chosen randomly from the interval $[-\theta_w, \theta_w]$ (the polycrystal is thus *anisotropic*, due to GBE processing, for $\theta_w < \pi/2$). For simplicity, the rotation axis, which is normal to the two-dimensional grains, is a two-fold symmetry axis. Then a facet is special if the misorientation of the adjacent grains is less than the threshold angle θ_t, which is related to the fraction of special facets by $p_s = (\theta_t/\theta_w) - (\theta_t/\theta_w)^2/4$ when $\theta_t < \pi - 2\theta_w$. This restriction on θ_t enables easy derivations (given in Appendix A) of the triple-junction probabilities p_i with $i=0,1,2,3$, while allowing essentially all cases of interest. For example, low-angle and high-angle boundaries in real materials are typically distinguished by a misorientation angle θ_t of 12° to 15°, while GBE processing has produced samples with p_s up to 0.7, corresponding to a ratio $\theta_t/\theta_w = 2[1-(1-p_s)^{1/2}] \approx 0.9$ in this model. Note that special facet fractions $p_s > 0.75$ cannot be attained without allowing $\theta_t > \theta_w$ (that is, without narrowing the angular spread of crystal orientations so that θ_w is less than the threshold angle θ_t). Analytical expressions for the triple-junction probabilities p_i as functions of the ratio θ_t/θ_w are presented in Table I and are plotted in Fig. 1. (These have been verified numerically, by counting triple junctions in computer-generated polycrystals.)

TABLE I. Analytical expressions for the fraction p_s of special facets and the triple-junction probabilities p_i ($i=0,1,2,3$), as functions of $\gamma \equiv \theta_t/\theta_w$. These are correct under the condition that $\theta_t < \pi - 2\theta_w$.

	$0 \leqslant \gamma \leqslant 1$	$1 \leqslant \gamma \leqslant 2$
p_s	$\gamma - \frac{1}{4}\gamma^2$	$\gamma - \frac{1}{4}\gamma^2$
p_0	$(1-\gamma)^3$	0
p_1	$3\gamma - \frac{9}{2}\gamma^2 + \frac{7}{4}\gamma^3$	$2 - 3\gamma + \frac{3}{2}\gamma^2 - \frac{1}{4}\gamma^3$
p_2	$\frac{3}{4}\gamma^2 - \frac{1}{2}\gamma^3$	$-1 + 3\gamma - \frac{9}{4}\gamma^2 + \frac{1}{2}\gamma^3$
p_3	$\frac{3}{4}\gamma^2 - \frac{1}{4}\gamma^3$	$\frac{3}{4}\gamma^2 - \frac{1}{4}\gamma^3$

Figure 2 shows the triple-junction probabilities p_i as functions of the fraction p_s of special facets, for both anisotropic correlated polycrystals (red curves) and random polycrystals (black curves). The curves are labeled by the i values 0, 1, 2, and 3, signifying the number of special facets belonging to a triple junction. For example, p_1 is the probability that an arbitrarily selected triple junction has one special facet and two nonspecial facets. The differences in the two sets of curves indicate that the number density of nonspecial double junctions (that is, p_1) *and clustering of those junctions* are significantly enhanced in the correlated polycrystals.

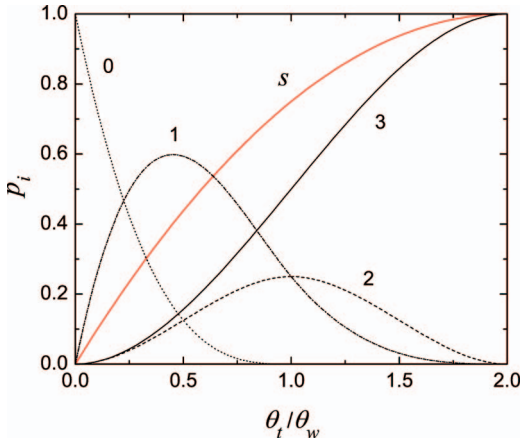

FIG. 1. (Color) Triple-junction probabilities p_i plotted against the ratio θ_t/θ_w. The curves are labeled by the i values 0, 1, 2, and 3, signifying the number of special facets belonging to a triple junction. For example, p_2 is the probability that an arbitrarily selected triple junction has two special facets and one nonspecial facet. The red curve labeled by s is the fraction p_s of special facets. The analytical expressions that produce these curves are given in Table I.

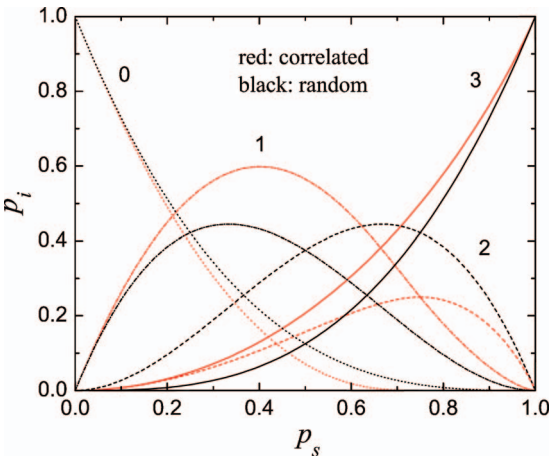

FIG. 2. (Color) Triple-junction probabilities p_i plotted against the fraction p_s of special facets, for both anisotropic correlated polycrystals (red curves) and random polycrystals (black curves). The curves are labeled by the i values 0, 1, 2, and 3, signifying the number of special facets belonging to a triple junction. For example, p_1 is the probability that an arbitrarily selected triple junction has one special facet and two nonspecial facets. The differences in the two sets of curves indicate that the number density of nonspecial double junctions (that is, p_1) *and clustering of those junctions* are significantly enhanced in the correlated polycrystals.

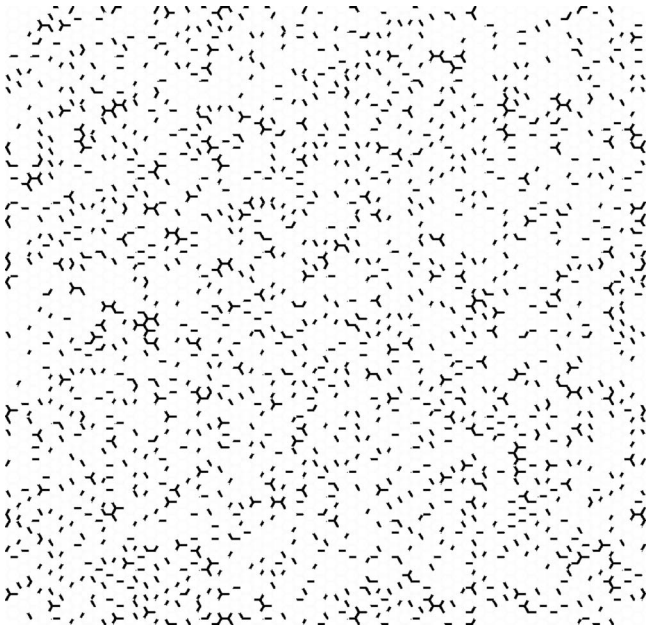

FIG. 3. Correlated polycrystal (3000 grains) with fraction of special facets $p_s=1/5$. Only the special facets are shown (black lines). The prevalence of special triple junctions (p_3) and isolated special facets apparent in this microstructure are predicted in Fig. 2.

tions of the fraction p_s of special facets, for both correlated and random polycrystals. Very similar curves have been obtained by Frary and Schuh[6] for their "fiber texture" microstructure. It is noteworthy that the p_1 and p_2 curves for the correlated polycrystals lie well above and below, respectively, the corresponding curves for the random polycrystals.

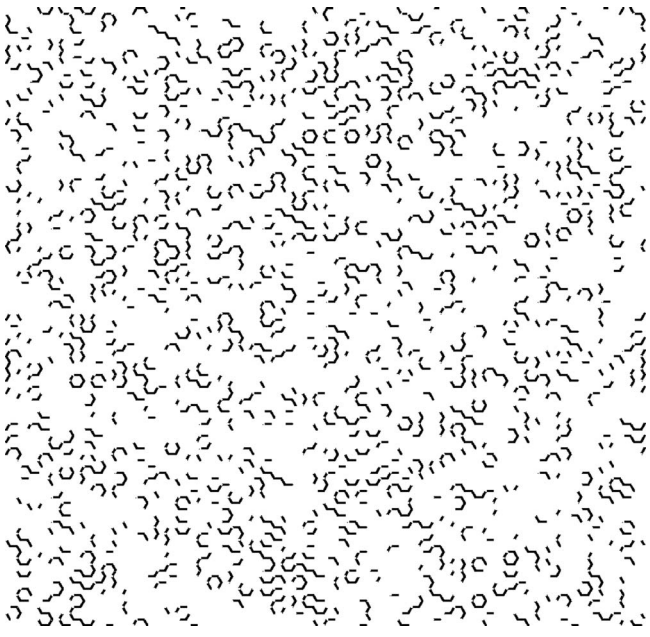

FIG. 4. Correlated polycrystal (3000 grains) with fraction of special facets $p_s=3/4$. Only the nonspecial facets are shown (black lines). The prevalence of nonspecial double junctions (p_1) and the clustering of those junctions, apparent in this microstructure, are predicted in Fig. 2.

TABLE II. Analytical expressions for the fraction p_s of special facets and the triple-junction probabilities p_i ($i=0,1,2,3$). The first two columns pertain to *isotropic* polycrystals (pre-GBE, so $\theta_w=\pi/2$), while the third (last) column pertains to a *random distribution* of special and nonspecial facets.

	$0\leqslant\theta_t\leqslant\pi/3$	$\pi/3\leqslant\theta_t\leqslant\pi/2$	Random
p_s	$2\theta_t/\pi$	$2\theta_t/\pi$	
p_0	$\left(1-\frac{3}{2}p_s\right)^2$	0	$(1-p_s)^3$
p_1	$3p_s\left(1-\frac{5}{4}p_s\right)$	$3(1-p_s)^2$	$3(1-p_s)^2p_s$
p_2	$\frac{3}{4}p_s^2$	$3(1-p_s)(2p_s-1)$	$3(1-p_s)p_s^2$
p_3	$\frac{3}{4}p_s^2$	$\frac{3}{4}p_s^2+\left(\frac{3}{2}p_s-1\right)^2$	p_s^3

The prevalence, in correlated polycrystals, of special triple junctions and isolated special facets, and of nonspecial double junctions, is obvious in Figs. 3 and 4 respectively. Clusters of special facets are seen to be ramified, while clusters of nonspecial facets are elongated (fiber like).

It is interesting to note that, in the absence of GBE processing (so the polycrystal is *isotropic*—that is, $\theta_w=\pi/2$), the fraction of special facets $p_s=2\theta_t/\pi$. Then $\theta_t=15°$ $(=\pi/12)$ produces $p_s=1/6$. The triple-junction probabilities p_i for the isotropic polycrystal are derived in Appendix B and presented in Table II.

The simulated polycrystal, represented by a regular network of grain boundaries with spatially varying elasticity modulus, will initially respond elastically to an applied stress or strain. However, as the stress or strain is increased, the inhomogeneity of the system will lead to sequential facet rupture and eventual catastrophic failure of the polycrystal. Because the stress and strain fields must be recalculated after every rupture, it is convenient to relate these by a *scalar* version of Hooke's law, $\sigma_{ij}=\mu_{ij}\epsilon_{ij}$ where σ_{ij} is the normal stress across the facet separating grains i and j, μ_{ij} is the elasticity modulus of that facet, and the strain $\epsilon_{ij}=u_i-u_j$ is the difference in displacements of the two adjacent grains. In this electrical analog, the system is mapped directly onto a triangular lattice of nodes (each centered on a grain) and conducting bonds (each perpendicular to a grain boundary facet). The conductance g_{ij} of a bond is the elasticity modulus μ_{ij} of the corresponding facet. Then an electrical potential difference applied across the triangular network corresponds to a strain applied to the polycrystal, so that the calculated potential ϕ_i at node i gives the displacement u_i of grain i, and the calculated current $j_{ij}=g_{ij}(\phi_i-\phi_j)$ through bond ij gives the local stress at facet ij. (Note that all stresses are normal to the grain boundaries in this scalar model.) In accordance with Ohm's law for an electrical circuit, the local stresses $\{\sigma_{ij}\}$ and strains $\{\epsilon_{ij}\}$ are distributed over the grain boundary network such that the total strain energy $\Sigma\sigma_{ij}\epsilon_{ij}/2$ is minimized.[8] Consistent with this minimization principle, a grain boundary facet will fail when its local strain energy

$\sigma_{ij}\epsilon_{ij}/2$ exceeds a specified threshold value. This rupture-criterion is in the spirit of the phenomenological Griffith model for microcrack nucleation.[9]

This treatment of stresses and strains in a 2D polycrystal is thus similar to that in other electrical "fuse" models of fracture or electrical breakdown.[10] The polycrystal model presented here differs from those mainly by the use and interpretation of results: for example, the stress-strain curves shown below do not have an electrical counterpart, and facet triple junctions, so important to the properties of polycrystals, do not have an analogous resistor network feature (in fact few fuse models use a triangular lattice). The long-standing popularity of fuse models of facture attests to the belief that the electrical analog (obeying the *scalar* Ohm's law) qualitatively reproduces stress and strain fields (related by the *vectoral* Hooke's law) such that damage properties can be profitably studied. [Of course, results obtained by a fuse model cannot be *quantitatively* correct: for example, Batrouni and Hansen[11] found the fracture surface roughness exponent for 3D random fuse networks to be much smaller than the experimental value for real materials, which they attribute to the scalar (versus vector) nature of their model.] Clearly, a next step is to apply finite element-based models[12] (with continuum constitutive laws) to polycrystals with special and nonspecial grain boundaries; in particular, this would remove the unrealistic constraint that stress is always normal to the grain boundaries.

It will be useful below to comment here on *random* polycrystals (so the distribution of special boundaries is *not* correlated). This honeycomb network (of special and nonspecial facets) is the *dual* of the regular triangular network (of conducting and insulating bonds). The percolation threshold (for the conducting bonds) of the latter is $p_c = 2\sin(\pi/18) \approx 0.3473$.[13] Thus the percolation threshold for the honeycomb network is $1-p_c$, which means that the nonspecial facets percolate when the fraction of special facets $p_s \leqslant p_c$. This bound is increased slightly in the case of *correlated* polycrystals, since there the nonspecial facets tend to form elongated clusters (due to the prevalence of nonspecial double junctions).

III. CALCULATIONS AND RESULTS

The basic procedure is to create a correlated polycrystalline microstructure, transform it to the corresponding electrical network, and solve the set of Kirchhoff equations (embodying Ohm's law) for the potential field $\{\phi_i\}$, given a *fixed* potential difference V applied across the system. The simulation proceeds by repeating the two-step process consisting of (1) breaking the bond ij with the largest value of the dissipation energy $g_{ij}(\phi_i - \phi_j)^2$ and (2) recalculating the potential field. Prior to breaking a bond, the total current I and largest local value E of the dissipation energy are recorded, thus giving the sequence $\{(I_n, E_n)\}$. The effective conductance G of the network and the total current I, which remain proportional to one another due to the relationship $V = I/G$, decline as bonds are broken.

The linear relationship between I and V enables a stress-strain curve to be constructed in the following manner. The value of the dissipation energy E_1 of the first bond to be broken is regarded as the critical energy density at which bonds subsequently break. It thus provides the scaling factors $\gamma_n = (E_1/E_n)^{1/2}$ used to convert the electrical quantities to points (ϵ, σ) on the stress-strain curve. Immediately *prior* to failure of the nth facet (bond), $(\epsilon, \sigma)_{pre} = (V_n^*, \gamma_n I_n)$, while immediately *after* failure of the nth facet, $(\epsilon, \sigma)_{post} = (V_n^*, \gamma_n I_{n+1})$, where $V_n^* = \max[\gamma_n V, V_{n-1}^*] = V \max[\gamma_n, \gamma_{n-1}, \ldots, \gamma_1]$ and $V_1^* = V$. Thus each facet failure contributes a *pair* of points to the stress-strain curve. [This calculation of V_n^* ensures that the strain is not decreased by a facet failure, but also has the effect that the point $(\epsilon_n, \sigma_n)_{pre}$ does not overlay the prior point $(\epsilon_{n-1}, \sigma_{n-1})_{post}$.] Note that only a few points will satisfy $(\epsilon, \sigma)_{pre} = (\gamma_n V, \gamma_n I_n)$; these indicate facet failures with $E_n < \min[E_{n-1}, E_{n-2}, \ldots, E_1]$ that may initiate an *avalanche* of subsequent facet failures at the strain $\gamma_n V$. An avalanche is a sequence of consecutive facet failures where the dissipation energy $E_n \geqslant \min[E_{n-1}, E_{n-2}, \ldots, E_1]$. The resulting stress-strain curve thus exhibits discontinuities where avalanches (or bursts) of facet failures occur prior to the final, catastrophic failure (which of course is a massive, highly localized avalanche).

Results are presented here for periodic (in the transverse direction) polycrystals having 3000 grains (so the 2D system forms a cylinder in 3D space, with the external strain applied in the direction of the cylinder axis) and fractions $p_s = 1/5, 1/3, 1/2, 3/4$ of special facets. In each case, separate simulations were performed using elasticity contrast values $\mu_s/\mu_{ns} = 10$ and 100 (the subscript *ns* refers to "nonspecial"), which are within a wide range of experimental measurements.[14]

Figures 5–12 show damage accumulation in eight representative microstructures (for the four values of p_s and the two values of μ_s/μ_{ns}). Nonspecial facets are indicated by black lines; these may be overlaid by heavy red or green lines, indicating a facet that ruptured prior to, or during, catastrophic failure, respectively. (Note that these figures are snapshots taken during, rather than after, the catastrophic failure event.)

For a given polycrystal, the response to the applied strain appears to depend primarily on whether its fraction $(1-p_s)$ of nonspecial facets is above or below the percolation threshold (for nonspecial facets)—that is, whether the special facet density p_s is below or above $p_c \approx 0.35$. In particular, microstructures in which the nonspecial facets do not percolate ($p_s = 1/2$ and $3/4$) are damaged by failure of *special* facets that connect clusters of nonspecial facets. These ruptures may occur in "bursts" (multiple failures at an applied strain), but in any case will create large, extended clusters of "weak" (nonspecial plus ruptured) facets. As applied strain is further increased, sufficient stress is diverted around or through a cluster of critical size that a crack is nucleated on the cluster and catastrophic failure of the polycrystal ensues. In contrast, microstructures in which the nonspecial facets do percolate ($p_s = 1/5$) are damaged by failure of *nonspecial* facets. It is easy to imagine (see Figs. 5 and 9) that the microstructure is comprised of *irregularly* shaped grains bounded by nonspecial facets (the black lines in the figures).

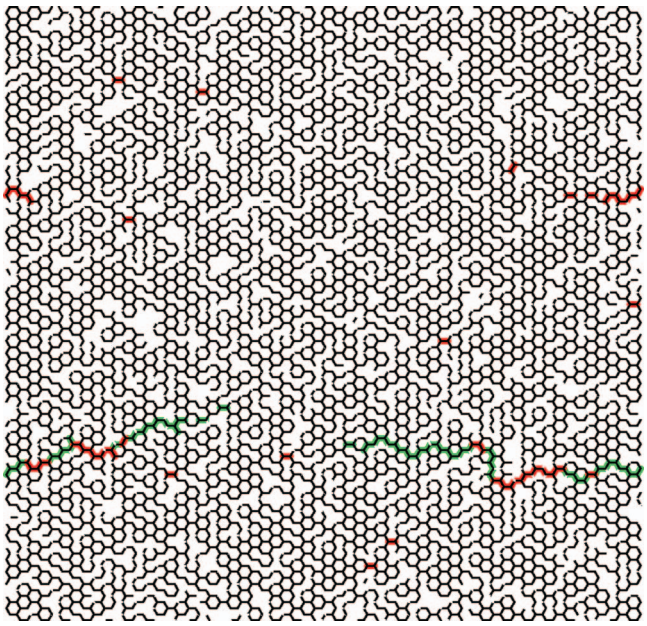

FIG. 5. (Color) Correlated polycrystal (3000 grains) with fraction of special facets $p_s=1/5$ and elasticity contrast $\mu_s/\mu_{ns}=100$. Note that all facet failures occurred at nonspecial facets. The avalanche sizes, in the order that the avalanches (red facets) occurred, are 3,1,1,1,2,1,1,1,1,7,2,3,1,1,4,1,20,1.

Then facet ruptures occur only between grains, and appear to be more likely to occur between two grains that are elongated in the direction of the applied field.

It should be emphasized that in both cases (the fraction of nonspecial facets is below or above the percolation threshold), the damage scenario is a consequence of the crystallographic constraint, as it produces an excess of nonspecial double junctions (triple junctions comprised of two nonspecial facets and one special facet) thereby creating fibrous clusters of nonspecial facets embedded in a special "matrix"

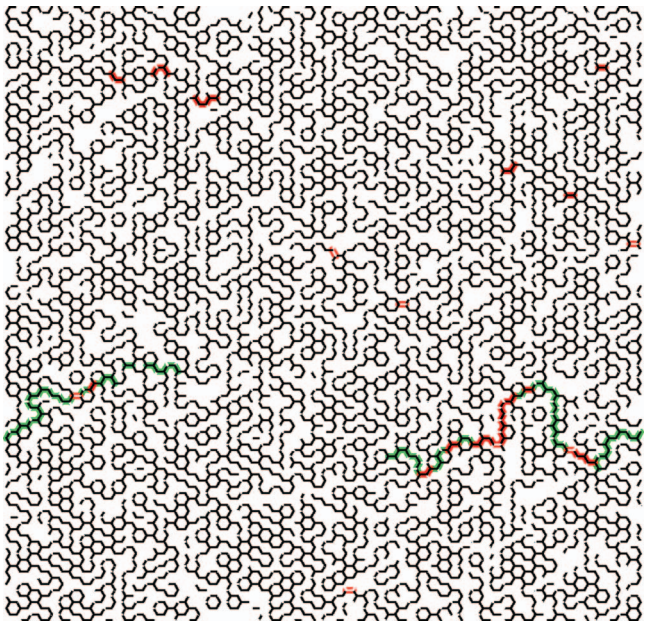

FIG. 6. (Color) Correlated polycrystal (3000 grains) with fraction of special facets $p_s=1/3$ and elasticity contrast $\mu_s/\mu_{ns}=100$. This microstructure is just above the percolation threshold for the non-special facets. The avalanche sizes, in the order that the avalanches (red facets) occurred, are 1,1,1,2,1,1,5,1,4,8,17,1.

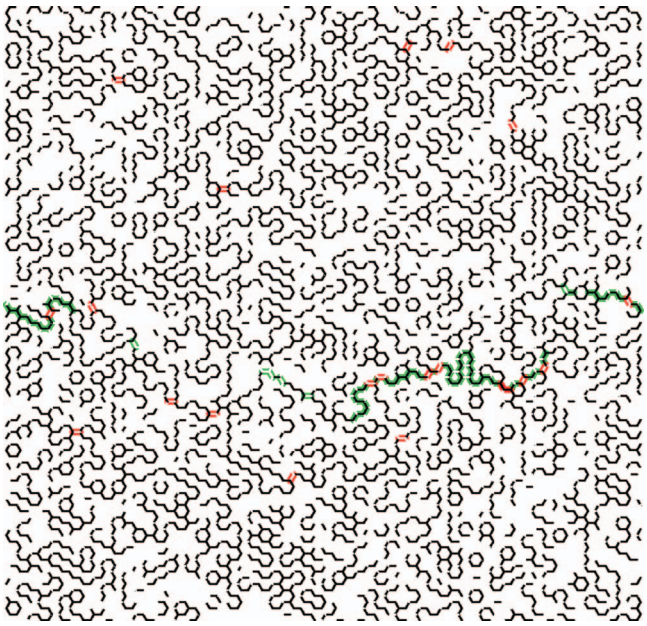

FIG. 7. (Color) Correlated polycrystal (3000 grains) with fraction of special facets $p_s=1/2$ and elasticity contrast $\mu_s/\mu_{ns}=100$. Note that nearly all the facet failures comprising avalanches (red facets) occurred at special facets, thereby creating elongated clusters of "weak" facets (nonspecial plus ruptured). The avalanche sizes, in the order that the avalanches occurred, are 2,1,1,2,2,1,1,1,1,1,1,7.

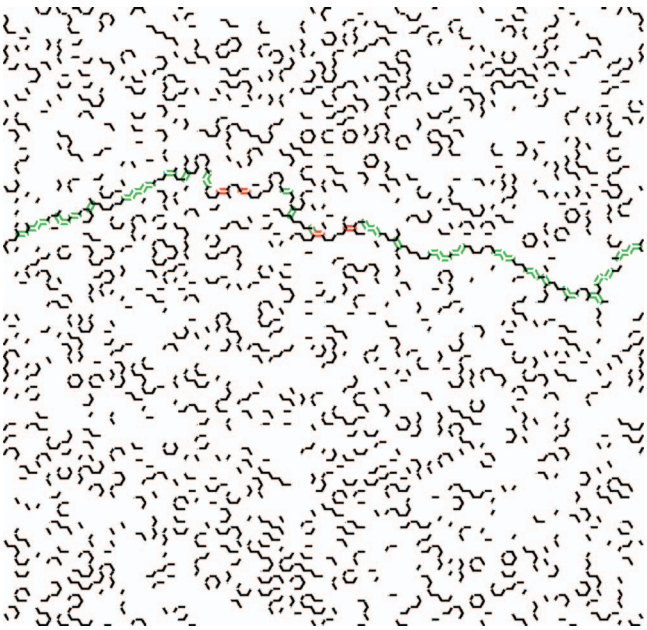

FIG. 8. (Color) Correlated polycrystal (3000 grains) with fraction of special facets $p_s=3/4$ and elasticity contrast $\mu_s/\mu_{ns}=100$. Note that all the facet failures (up to this point) have occurred at special facets, thereby creating elongated clusters of "weak" facets (nonspecial plus ruptured). Only a single avalanche (red facets), of size 4, preceded the catastrophic failure event (green facets).

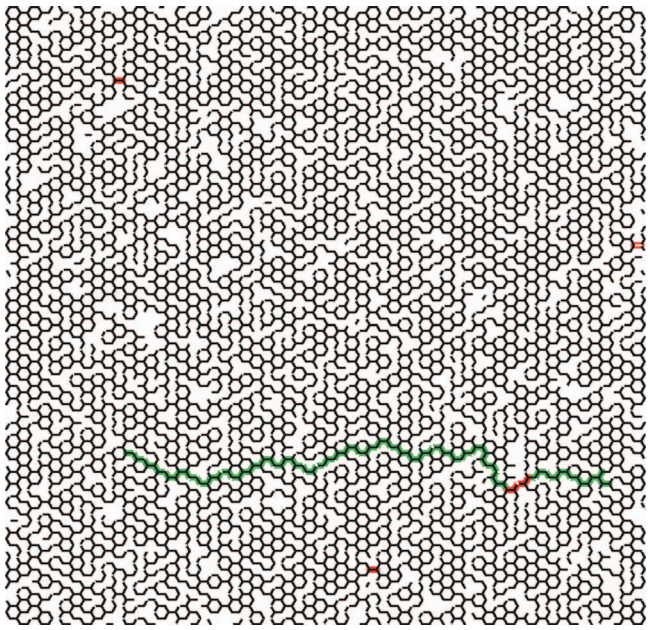

FIG. 9. (Color) Correlated polycrystal (3000 grains) with fraction of special facets $p_s=1/5$ and elasticity contrast $\mu_s/\mu_{ns}=10$. The avalanche sizes, in the order that the avalanches (red facets) occurred, are 1,1,2,1,1,1.

in the first case, or imposing a coarse, granular structure defined by nonspecial grain boundaries in the second case.

The damage evolution is less predictable when the fraction of nonspecial facets is near the percolation threshold ($p_s=1/3$). Percolation effects are less pronounced as the elasticity contrast μ_s/μ_{ns} decreases, which perhaps accounts

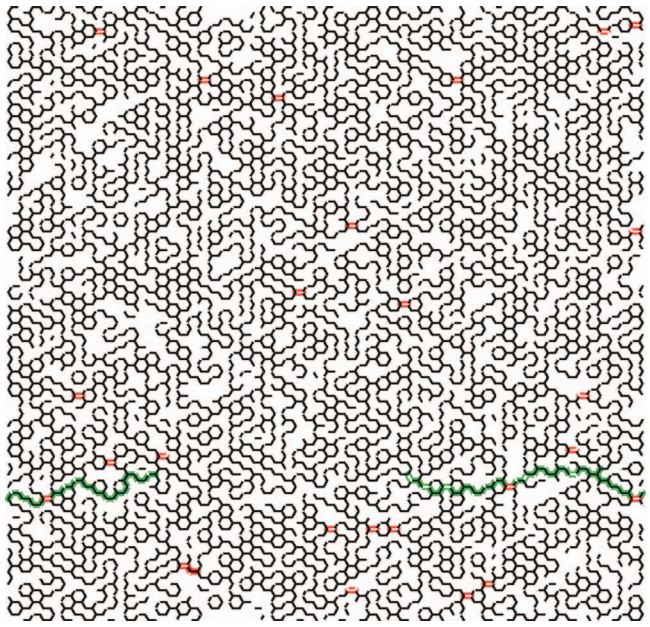

FIG. 10. (Color) Correlated polycrystal (3000 grains) with fraction of special facets $p_s=1/3$ and elasticity contrast $\mu_s/\mu_{ns}=10$. This microstructure is just above the percolation threshold for the nonspecial facets. The avalanche sizes, in the order that the avalanches (red facets) occurred, are 2,1,1,1,1,3,1,3,1,1,3,1,1.1,2,1,1,2.

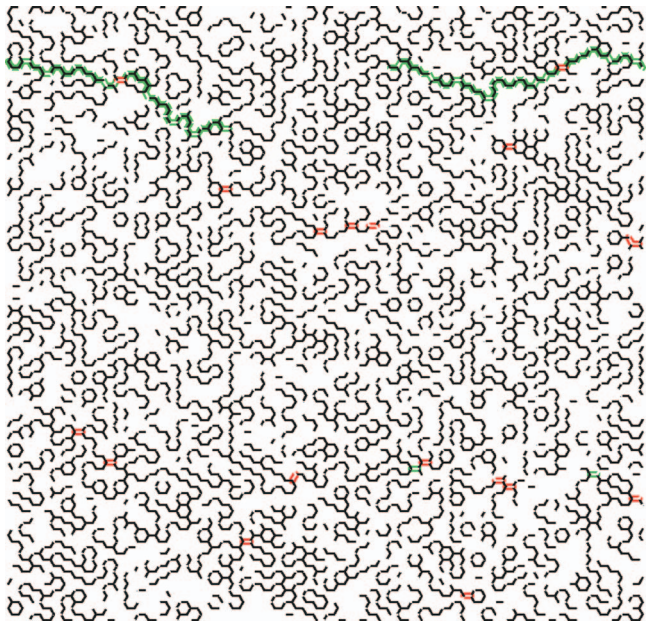

FIG. 11. (Color) Correlated polycrystal (3000 grains) with fraction of special facets $p_s=1/2$ and elasticity contrast $\mu_s/\mu_{ns}=10$. Note that all the facet failures comprising avalanches (red facets) occurred at special facets, thereby creating elongated clusters of "weak" facets (nonspecial plus ruptured). The avalanche sizes, in the order that the avalanches occurred, are 1,1,1,2,1,7,1,1,3.

for the resemblance in the damage exhibited by the microstructures with $p_s=1/3$ and $1/2$ when $\mu_s/\mu_{ns}=10$ (Figs. 10 and 11). In contrast, the damage exhibited by the microstructure with $p_s=1/3$ and $\mu_s/\mu_{ns}=100$ (Fig. 6) appears to be a

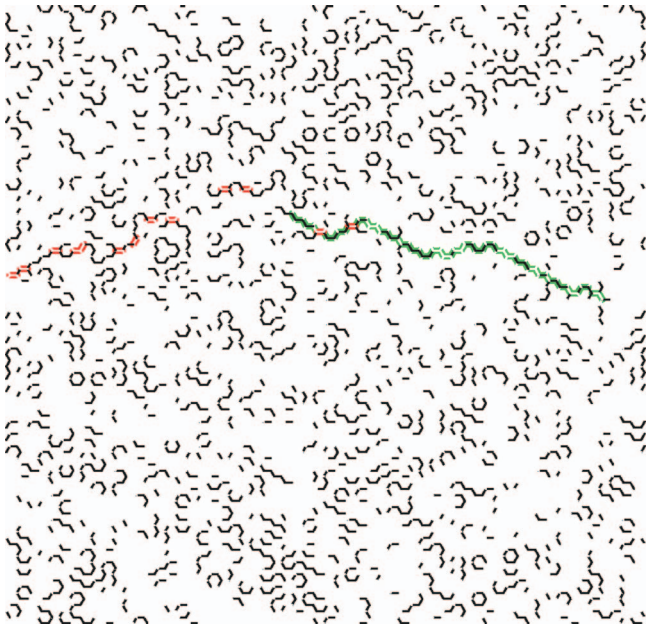

FIG. 12. (Color) Correlated polycrystal (3000 grains) with fraction of special facets $p_s=3/4$ and elasticity contrast $\mu_s/\mu_{ns}=10$. Note that the avalanches (red facets) of special-facet failures are highly localized, thereby creating a weakened zone at which the catastrophic failure event (green facets) takes place. The avalanche sizes, in the order that the avalanches occurred, are 2,2,2,7.

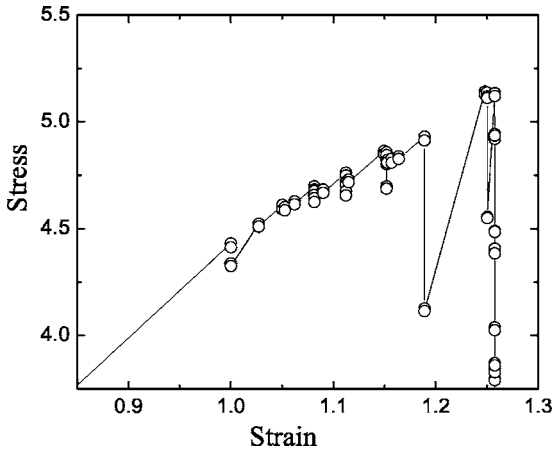

FIG. 13. Stress-strain curve for the correlated polycrystal shown in Fig. 10 (fraction of special facets $p_s=1/3$ and elasticity contrast $\mu_s/\mu_{ns}=10$). The discontinuities are due to avalanches of single-facet failures that occur as the applied stress or strain is increased.

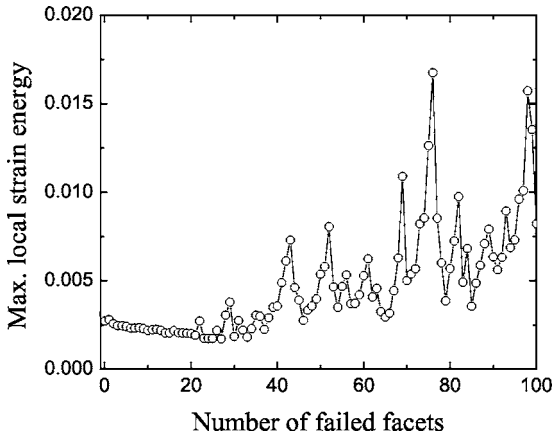

FIG. 14. Data used to generate the stress-strain curve in Fig. 13 (see text). The ordinate is the largest element of the set $\{\sigma_{ij}\epsilon_{ij}/2\}_n$ of local strain energies (the subscript n indicates that $n-1$ facets have failed to this point), calculated for a *fixed* applied strain of 1 (thus the ordinate is the dissipation energy E_n mentioned in the text). The facet corresponding to that largest value is the next (and nth) to fail.

combination of that seen in microstructures away from the percolation threshold (Figs. 5 and 7).

All these snapshots show the microstructure in the middle of the catastrophic failure event, before one end of the primary crack influences the behavior of the other. It is interesting to speculate whether the final crack path is, or approximates, a "critical manifold" as introduced by Meinke *et al.*[15] and applied to model polycrystals with randomly distributed special grain boundaries by McGarrity *et al.*[16] In that case high and low values of cohesive energy are assigned to special and nonspecial boundaries, respectively; then the critical manifold is the *global* minimum energy surface (or curve in 2D). This surface may resemble those formed by brittle, intergranular fracture of a polycrystalline material. In contrast, the present work emphasizes the *local* nature of damage and of crack nucleation and growth (for example, each facet failure alters the local stress and strain fields). That said, it would be interesting to obtain the critical manifolds for these microstructures prior to the first facet failure, where the global quantity to be minimized is the sum $\Sigma(E_1-\sigma_{ij}\epsilon_{ij}/2)$ for a connected, linear cluster of facets spanning the system.

A typical stress-strain curve is shown in Fig. 13, for the correlated polycrystal with $p_s=1/3$ and $\mu_s/\mu_{ns}=10$ (Fig. 10). Those points are calculated by the procedure described above, using the set $\{E_n\}$ of (unscaled) maximum local strain energies taken from Fig. 14. The smallest E value defines the onset of catastrophic failure; in general, the preceding E values in the sequence decrease fairly smoothly, while the succeeding E values vary wildly.

The discontinuities in the stress-strain curves prior to catastrophic failure indicate avalanches of spatially dispersed, single-facet failures. Electrical fuse models exhibit similar avalanches (of circuit element failures, in that case),[10] due to the heterogeneity of the network. Unfortunately the systems considered here are too small and too few in number to usefully speculate about avalanche size distributions. However, it should be noted that most avalanches observed in these simulations were quite small (one to five facets or so), except occasionally a larger avalanche of dispersed, single-facet failures would occur prior to or as part of the catastrophic failure event (i.e., the avalanche would induce crack nucleation and growth). This suggests that these polycrystalline systems are too small to support very large avalanches. The sizes of the avalanches apparent in Figs. 5–12 are given in the figure captions by a sequence of numbers, the nth number being the size (in number of single-facet failures) of the nth avalanche.

It is striking that for both random and correlated systems, the probability distribution of local strain energies $\{\sigma_{ij}\epsilon_{ij}/2\}$ decays (approximately) exponentially, with a few higher energy "outliers" (points beyond the exponential tail), even as damage proceeds. An example is shown in Fig. 15, which is again for the correlated polycrystal with $p_s=1/3$ and $\mu_s/\mu_{ns}=10$ (Fig. 10). According to the facet failure criterion, the facet corresponding to the furthest outlier (greatest strain energy) is next to fail. An avalanche occurs when redistribution of the total strain energy produces outliers with greater local strain energy than that of the smallest prior outlier. Typically, avalanches remove the outliers that are present initially (before any facet failures, as indicated by the black open circles in Fig. 15), leaving unaffected the exponential distribution of large local strain energies. Evidently those initial outliers correspond to "hot spots" in the system whose removal does not concentrate strain energy elsewhere (in this regard the system at first resembles the democratic fiber bundle model). However, when a facet corresponding to a point in the exponential tail is ruptured, catastrophic failure ensues, as new outliers (points beyond the exponential tail) are produced with every subsequent facet failure. In this respect the exponential distribution of large local strain energies represents a critical state: failure of a single facet from that distribution causes catastrophic failure of the system.

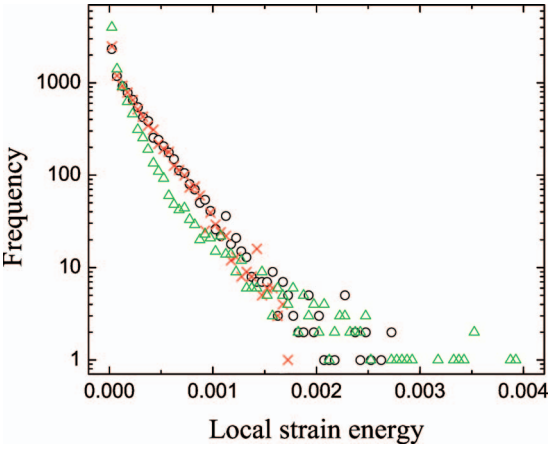

FIG. 15. (Color) Frequency of occurrence (i.e., unnormalized probability distribution) of local strain energies for the correlated polycrystal shown in Fig. 10 (fraction of special facets $p_s=1/3$ and elasticity contrast $\mu_s/\mu_{ns}=10$). The black circles indicate the initial (prior to any facet failures) distribution, the red crosses indicate the distribution immediately prior to catastrophic failure (only the red facets in Fig. 10 have failed), and the green triangles indicate the distribution after the catastrophic failure event is well underway (all red and green facets in Fig. 10 have failed). A number of green triangles lie outside the plot at higher strain energies ($\geqslant 0.004$).

IV. CONCLUDING REMARKS

The simple, two-dimensional model polycrystal presented here is an array of hexagonal grains, each distinguished by a crystallographic orientation taken randomly from a distribution. This permits assignment of special or nonspecial properties to each grain boundary facet according to the degree of misorientation across the facet. The "crystallographic constraint" (namely, that the misorientation angles around a triple junction must sum to 360°) produces nonrandom distributions of the various types of grain triple junctions—most importantly, an enhanced density of triple junctions where two nonspecial boundaries connect with a single special boundary.

Because mechanical properties are of interest here, special and nonspecial facets are assigned high and low values, respectively, of the elasticity modulus. The polycrystal is then effectively a honeycomb network of grain boundary facets, where the distribution of special and nonspecial facets is spatially correlated due to the crystallographic constraint.

The stress and strain fields for the polycrystal under an applied strain are assumed to satisfy a scalar Hooke's law. They are obtained by solving the electrical analog to this problem on the triangular network of conducting bonds that is the dual to the honeycomb network of facets. The electrical analog provides a facet failure criterion, so a series of calculations produces a sequence of facet failures. The linearity of the scalar laws allows stress-strain curves to be constructed, which in turn allows the sequences of facet failures to be revealed as avalanches and catastrophic failure events (crack nucleation and growth).

The damage evolution is found to be affected by the spatial correlation of special and nonspecial facets—in particular, by the prevalence of nonspecial double junctions. These form elongated, weak "fibers" in polycrystals having a high fraction of special facets, and weak boundaries defining irregularly shaped grains in polycrystals having a low fraction of special facets. In either case the clustering of nonspecial double junctions is detrimental to the mechanical properties of the polycrystals.

A recent experiment[17] has shown how to *monitor* creep damage by combined and continuous x-ray microtomography and x-ray diffraction. Perhaps this approach can be taken to distinguish avalanches of single-facet failures and the localization of damage that results in catastrophic failure. The 2D model presented here suggests that polycrystals with a low fraction of special boundaries (pre-GBE) will exhibit more homogeneous and extensive damage prior to catastrophic failure, while polycrystals with a high fraction of special boundaries (post-GBE) will exhibit more localized damage prior to catastrophic failure.

ACKNOWLEDGMENT

This work was supported in part by the INL Laboratory Directed Research and Development Program under DOE Idaho Operations Office Contract No. DE-AC07-05ID14517.

APPENDIX A: DERIVATION OF TRIPLE-JUNCTION PROBABILITIES FOR ANISOTROPIC POLYCRYSTALS

The derivations follow from three conditions: (1) the rotation axis normal to each two-dimensional, hexagonal grain is a twofold symmetry axis; (2) the crystallographic orientations of the grains lie randomly within the angular interval $[-\theta_w, \theta_w]$; and (3) the threshold angle θ_t satisfies the relation $\theta_t < \pi - 2\theta_w$. The first condition says that a grain with crystallographic orientation θ is indistinguishable from a grain with orientation $\theta \pm \pi$. The third condition greatly simplifies the derivations by avoiding a complication that will be noted below and, in any event, is not a practical limitation since GBE is intended to decrease θ_w to a small value.

In what follows, the crystallographic orientations of the three grains meeting at a triple junction are designated θ_i with $i=1,2,3$. These angles are measured with respect to a common direction and so can take on positive and negative values within the interval $[-\theta_w, \theta_w]$.

1. Derivation of p_s when $\theta_t \leqslant \theta_w$

The fraction p_s of special facets equals the probability that (i) $|\theta_1 - \theta_2| \leqslant \theta_t$, or that (ii) $|\theta_1 - \theta_2| > \theta_t$ but $\pi - |\theta_1 - \theta_2| \leqslant \theta_t$, for an *arbitrarily selected* pair of (adjacent) grains. Scenario (ii) greatly complicates the mathematics and so will be ignored by imposing the (third) condition $\theta_t < \pi - 2\theta_w$. Then considering only scenario (i), p_s equals the probability that grain 1 has orientation θ_1, multiplied by the probability that the orientation of grain 2 (that is, θ_2) lies within θ_t of θ_1, integrated over all possible values of θ_1 (that is, over the interval $[-\theta_w, \theta_w]$). Expressed mathematically, this is

$$p_s = \int_{-\theta_w}^{\theta_w} \frac{d\theta_1}{2\theta_w} \times \begin{pmatrix} \dfrac{\theta_t + (\theta_w + \theta_1)}{2\theta_w} & \text{for } \theta_1 \leqslant -\theta_w + \theta_t \\ \dfrac{2\theta_t}{2\theta_w} & \text{for } -\theta_w + \theta_t \leqslant \theta_1 \leqslant \theta_w - \theta_t \\ \dfrac{\theta_t + (\theta_w - \theta_1)}{2\theta_w} & \text{for } \theta_1 \geqslant \theta_w - \theta_t \end{pmatrix}. \tag{A1}$$

Performing the three integrations over the angular segments $[-\theta_w, -\theta_w + \theta_t]$, $[-\theta_w + \theta_t, \theta_w - \theta_t]$, and $[\theta_w - \theta_t, \theta_w]$ gives the result

$$p_s = \frac{\theta_t}{\theta_w} - \frac{1}{4}\left(\frac{\theta_t}{\theta_w}\right)^2. \tag{A2}$$

2. Derivation of p_s when $\theta_w \leqslant \theta_t \leqslant 2\theta_w$

In this case,

$$p_s = \int_{-\theta_w}^{\theta_w} \frac{d\theta_1}{2\theta_w} \times \begin{pmatrix} \dfrac{\theta_t + (\theta_w + \theta_1)}{2\theta_w} & \text{for } \theta_1 \leqslant \theta_w - \theta_t \\ 1 & \text{for } \theta_w - \theta_t \leqslant \theta_1 \leqslant -\theta_w + \theta_t \\ \dfrac{\theta_t + (\theta_w - \theta_1)}{2\theta_w} & \text{for } \theta_1 \geqslant -\theta_w + \theta_t \end{pmatrix}, \tag{A3}$$

which produces the same result.

3. Derivation of p_3

Arbitrarily select a triple junction, and arbitrarily assign the labels 1, 2, and 3 to the three grains. Then p_3 is *proportional* to the probability that grain 1 has orientation θ_1; multiplied by the probability that the orientations of grains 2 and 3 are such that $\theta_2 \geqslant \theta_1$ and $\theta_3 \geqslant \theta_1$, and furthermore both lie within $[\theta_1, \theta_1 + \theta_t]$ (that is, within θ_t of θ_1); integrated over all possible values of θ_1. The proportionality constant is 3, which is the number of ways of assigning the label 1 to the three grains. Expressed mathematically, this is

$$p_3 = 3\int_{-\theta_w}^{\theta_w} \frac{d\theta_1}{2\theta_w} \times \begin{pmatrix} \dfrac{\theta_t}{2\theta_w} & \dfrac{\theta_t}{2\theta_w} & \text{for } \theta_1 \leqslant \theta_w - \theta_t \\ \dfrac{\theta_w - \theta_1}{2\theta_w} & \dfrac{\theta_w - \theta_1}{2\theta_w} & \text{for } \theta_1 \geqslant \theta_w - \theta_t \end{pmatrix}. \tag{A4}$$

Performing the two integrations gives the result

$$p_3 = \frac{3}{4}\left(\frac{\theta_t}{\theta_w}\right)^2 - \frac{1}{4}\left(\frac{\theta_t}{\theta_w}\right)^3. \tag{A5}$$

4. Derivation of p_0

Arbitrarily select a triple junction, and arbitrarily assign the labels 1, 2, and 3 to the three grains. Then p_0 is *proportional* to the probability that grain 1 has orientation θ_1, multiplied by the probability that the orientation of grain 2 is such that $\theta_2 \leqslant \theta_1$ and furthermore lies within $[-\theta_w, \theta_1 - \theta_t)$ (that is, at least θ_t *away* from θ_1), multiplied by the probability that the orientation of grain 3 is such that $\theta_3 \geqslant \theta_1$ and furthermore lies within $(\theta_1 + \theta_t, \theta_w]$ (that is, at least θ_t *away* from θ_1), integrated over all possible values of θ_1. (So the boundary between grains 1 and 2, and the boundary between grains 1 and 3, are both *non-special* facets.) The proportionality constant is 6, which is the number of ways of assigning the labels to the three grains. Clearly $p_0 = 0$ in the case $\theta_w \leqslant \theta_t \leqslant 2\theta_w$, since the condition that θ_2 and θ_3 lie within $[-\theta_w, \theta_w]$ precludes the possibility that $|\theta_2 - \theta_3| > 2\theta_t$. For the case $\theta_t \leqslant \theta_w$,

$$p_0 = 6\int_{-\theta_w}^{\theta_w} \frac{d\theta_1}{2\theta_w} \begin{pmatrix} 0 & \dfrac{\theta_w - \theta_1 - \theta_t}{2\theta_w} & \text{for } \theta_1 \leqslant -\theta_w + \theta_t \\ \dfrac{\theta_w + \theta_1 - \theta_t}{2\theta_w} & \dfrac{\theta_w - \theta_1 - \theta_t}{2\theta_w} & \text{for } -\theta_w + \theta_t \leqslant \theta_1 \leqslant \theta_w - \theta_t \\ \dfrac{\theta_w + \theta_1 - \theta_t}{2\theta_w} & 0 & \text{for } \theta_1 \geqslant \theta_w - \theta_t \end{pmatrix} = 6\int_{-\theta_w + \theta_t}^{\theta_w - \theta_t} \frac{d\theta_1}{2\theta_w} \frac{\theta_w + \theta_1 - \theta_t}{2\theta_w} \frac{\theta_w - \theta_1 - \theta_t}{2\theta_w}, \tag{A6}$$

which gives the result

$$p_0 = \left(1 - \frac{\theta_t}{\theta_w}\right)^3. \tag{A7}$$

5. Derivation of p_1 when $\theta_t \leqslant \theta_w$

Arbitrarily select a triple junction, and arbitrarily assign the labels 1, 2, and 3 to the three grains. Then p_1 is *proportional* to the probability that grain 1 has orientation θ_1, multiplied by the probability that the orientation of grain 2 is

such that $\theta_2 \leqslant \theta_1$ and furthermore lies within $[\theta_1-\theta_t, \theta_1]$ (that is, within θ_t of θ_1), multiplied by the probability that the orientation of grain 3 is such that $\theta_3 \geqslant \theta_1$ and furthermore lies within $(\theta_1+\theta_t, \theta_w]$ (that is, at least θ_t *away* from θ_1), integrated over all possible values of θ_1. (So the boundary between grains 1 and 2 is a *special* facet and the boundary between grains 1 and 3 is a *nonspecial* facet.) The proportionality constant is $2\times 6=12$, where the factor 2 accounts for the (identical) probability that, for a particular assignment of grain labels, the boundary between grains 1 and 2 is nonspecial (rather than special) and the boundary between grains 1 and 3 is special (rather than nonspecial), and 6 is the number of ways of assigning the labels to the three grains. Expressed mathematically, this is

$$p_1 = 12\int_{-\theta_w}^{\theta_w} \frac{d\theta_1}{2\theta_w} \begin{pmatrix} \dfrac{\theta_w+\theta_1}{2\theta_w} & \dfrac{\theta_w-\theta_1-\theta_t}{2\theta_w} & \text{for } \theta_1 \leqslant -\theta_w+\theta_t \\ \dfrac{\theta_t}{2\theta_w} & \dfrac{\theta_w-\theta_1-\theta_t}{2\theta_w} & \text{for } -\theta_w+\theta_t \leqslant \theta_1 \leqslant \theta_w-\theta_t \\ \dfrac{\theta_t}{2\theta_w} & 0 & \text{for } \theta_1 \geqslant \theta_w-\theta_t \end{pmatrix}, \tag{A8}$$

which gives the result

$$p_1 = 3\frac{\theta_t}{\theta_w} - \frac{9}{2}\left(\frac{\theta_t}{\theta_w}\right)^2 + \frac{7}{4}\left(\frac{\theta_t}{\theta_w}\right)^3. \tag{A9}$$

6. Derivation of p_1 when $\theta_w \leqslant \theta_t \leqslant 2\theta_w$

In this case,

$$p_1 = 12\int_{-\theta_w}^{\theta_w} \frac{d\theta_1}{2\theta_w} \begin{pmatrix} \dfrac{\theta_w+\theta_1}{2\theta_w} & \dfrac{\theta_w-\theta_1-\theta_t}{2\theta_w} & \text{for } \theta_1 \leqslant \theta_w-\theta_t \\ & 0 & \text{for } \theta_1 \geqslant \theta_w-\theta_t \end{pmatrix}, \tag{A10}$$

which gives the result

$$p_1 = 2 - 3\frac{\theta_t}{\theta_w} + \frac{3}{2}\left(\frac{\theta_t}{\theta_w}\right)^2 - \frac{1}{4}\left(\frac{\theta_t}{\theta_w}\right)^3. \tag{A11}$$

7. Derivation of p_2

The probability p_2 is most easily obtained from the relation $1=p_0+p_1+p_2+p_3$. Thus, in the case $\theta_t \leqslant \theta_w$,

$$p_2 = \frac{3}{4}\left(\frac{\theta_t}{\theta_w}\right)^2 - \frac{1}{2}\left(\frac{\theta_t}{\theta_w}\right)^3, \tag{A12}$$

and in the case $\theta_w \leqslant \theta_t \leqslant 2\theta_w$,

$$p_2 = -1 + 3\frac{\theta_t}{\theta_w} - \frac{9}{4}\left(\frac{\theta_t}{\theta_w}\right)^2 + \frac{1}{2}\left(\frac{\theta_t}{\theta_w}\right)^3. \tag{A13}$$

8. Comments on the p_i functions

It may be noted that the expressions above satisfy the relation $p_s=\frac{1}{3}p_1+\frac{2}{3}p_2+p_3$. Additional relations of interest are (1) $\frac{1}{3}p_2+p_3$ is the probability that both facets of an arbitrarily selected pair of connected facets are special and (2) $p_0+\frac{1}{3}p_1$ is the probability that both facets of an arbitrarily selected pair of connected facets are nonspecial. Substituting into relation (1) shows $\frac{1}{3}p_2+p_3 > p_s^2$, in contrast to the cases of random (uncorrelated) polycrystals and isotropic (correlated) polycrystals where $\frac{1}{3}p_2+p_3=p_s^2$. This different result is due to the restriction on the possible crystallographic orientations of the grains in an anisotropic polycrystal, which introduces the additional term $-\frac{1}{4}\left(\frac{\theta_t}{\theta_w}\right)^2$ in the expression for p_s.

9. Clustering of special and nonspecial facets

An interesting aspect of the derivations above is that in every case an integration is performed over all possible crystallographic orientations of grain 1. This suggests that probability functions (that is, number densities) can be straightforwardly obtained for any facet cluster comprised of facets belonging to the six triple junctions surrounding an arbitrarily selected grain (that is, grain 1). For example, arbitrarily select a grain (call it grain 1), and then arbitrarily select two of its six facets. Then the probability p_2' that both those facets are special is the probability that grain 1 has orientation θ_1, multiplied by the probability that the orientation of grain $2'$ (that is, θ_2) lies within θ_t of θ_1, multiplied by the probability that the orientation of grain $3'$ (that is, θ_3) lies within θ_t of θ_1, integrated over all possible values of θ_1. Thus, in the case $\theta_t \leqslant \theta_w$,

$$p_2' = \int_{-\theta_w}^{\theta_w} \frac{d\theta_1}{2\theta_w} \times \begin{pmatrix} \left[\frac{\theta_t + (\theta_w + \theta_1)}{2\theta_w}\right]^2 & \text{for } \theta_1 \leqslant -\theta_w + \theta_t \\ \left[\frac{2\theta_t}{2\theta_w}\right]^2 & \text{for } -\theta_w + \theta_t \leqslant \theta_1 \leqslant \theta_w - \theta_t \\ \left[\frac{\theta_t + (\theta_w - \theta_1)}{2\theta_w}\right]^2 & \text{for } \theta_1 \geqslant \theta_w - \theta_t \end{pmatrix} = \left(\frac{\theta_t}{\theta_w}\right)^2 - \frac{5}{12}\left(\frac{\theta_t}{\theta_w}\right)^3. \tag{A14}$$

It is interesting that this last result equals $\frac{1}{3}p_2 + p_3$, which, as noted above, is greater than p_s^2. This indicates that the special or nonspecial assignments of any two facets belonging to a grain are not independent and, by extension, that the special or nonspecial assignments of *any two* facets in the polycrystal are not independent. Thus the correlation length of the polycrystal equals the size of the polycrystal.

Number densities of larger facet clusters (that include facets beyond those comprising the triple junctions surrounding grain 1) may be found by use of nested integrals.

APPENDIX B: DERIVATION OF TRIPLE-JUNCTION PROBABILITIES FOR ISOTROPIC POLYCRYSTALS

These derivations follow from two conditions: (1) the rotation axis normal to each two-dimensional, hexagonal grain is a twofold symmetry axis, and (2) the crystallographic orientations of the grains are randomly chosen. As the first condition says that a grain with crystallographic orientation θ is indistinguishable from a grain with orientation $\theta + \pi$, it is convenient to restrict θ to lie within the angular interval $[-\pi/2, \pi/2]$. A further convenience is to choose (since the polycrystal is isotropic) the orientation of grain 1 to be $\theta_1 = 0$. It is then immediately apparent that the fraction of special facets $p_s = 2\theta_t/\pi$.

1. Derivation of p_3 when $\theta_t \leqslant \pi/3$

The function p_3 equals the probability that the crystallographic orientation θ_2 of grain 2 lies within $[-\theta_t, \theta_t]$ (that is, within θ_t of θ_1), multiplied by the probability $(2\theta_t - |\theta_2|)/\pi$ that the orientation θ_3 of grain 3 lies within $[-\theta_t, \theta_t]$ (that is, within θ_t of θ_1) *and* within $[\theta_2 - \theta_t, \theta_2 + \theta_t]$ (that is, within θ_t of θ_2), integrated over all possible values of θ_2. Expressed mathematically, this is

$$p_3 = \int_{-\theta_t}^{\theta_t} \frac{d\theta_2}{\pi} \begin{pmatrix} \frac{(\theta_t + \theta_2) + \theta_t}{\pi} & \text{for } \theta_2 \leqslant 0 \\ \frac{(\theta_t - \theta_2) + \theta_t}{\pi} & \text{for } \theta_2 \geqslant 0 \end{pmatrix}, \tag{B1}$$

which gives the result

$$p_3 = 3\left(\frac{\theta_t}{\pi}\right)^2 = \frac{3}{4}p_s^2. \tag{B2}$$

2. Derivation of p_3 when $\pi/3 \leqslant \theta_t \leqslant \pi/2$

There is an *additional* contribution to p_3 when both θ_t and $|\theta_2|$ are large, due to the probability $(2\theta_t - \pi + |\theta_2|)/\pi$ that the orientation θ_3 of grain 3 lies within θ_t of θ_1 (that is, within $[-\theta_t, \theta_t]$) *and* within θ_t of $\theta_2 + \pi$. This is

$$p_3^+ = \int_{-\theta_t}^{\theta_t} \frac{d\theta_2}{\pi} \times \begin{pmatrix} \frac{2\theta_t - \pi - \theta_2}{\pi} & \text{for } \theta_2 \leqslant -\pi + 2\theta_t \\ 0 & \text{for } -\pi + 2\theta_t \leqslant \theta_2 \leqslant \pi - 2\theta_t \\ \frac{2\theta_t - \pi + \theta_2}{\pi} & \text{for } \theta_2 \geqslant \pi - 2\theta_t \end{pmatrix}, \tag{B3}$$

which gives the result

$$p_3^+ = \left(\frac{3\theta_t - \pi}{\pi}\right)^2 = \left(\frac{3}{2}p_s - 1\right)^2. \tag{B4}$$

3. Derivation of p_0 when $\theta_t \leqslant \pi/4$

The function p_0 equals the probability that the crystallographic orientation θ_2 of grain 2 lies outside $[-\theta_t, \theta_t]$ (that is, at least θ_t away from θ_1), multiplied by the probability p' that the orientation θ_3 of grain 3 lies outside $[-\theta_t, \theta_t]$ (that is, at least θ_t away from θ_1) *and* at least θ_t away from both θ_2 and $\theta_2 + \pi$, integrated over all possible values of θ_2. The probability $p' = (\pi - 4\theta_t)/\pi$ when $|\theta_2| \geqslant 2\theta_t$, and $p' = (\pi - 2\theta_t - |\theta_2|)/\pi$ when $\theta_t < |\theta_2| \leqslant 2\theta_t$. Expressed mathematically, this is

$$p_0 = \int_{-\pi/2}^{\pi/2} \frac{d\theta_2}{\pi} \begin{pmatrix} \frac{\pi - 4\theta_t}{\pi} & \text{for } \theta_2 \leqslant -2\theta_t \\ \frac{\pi - 2\theta_t + \theta_2}{\pi} & \text{for } -2\theta_t \leqslant \theta_2 \leqslant -\theta_t \\ 0 & \text{for } -\theta_t \leqslant \theta_2 \leqslant \theta_t \\ \frac{\pi - 2\theta_t - \theta_2}{\pi} & \text{for } \theta_t \leqslant \theta_2 \leqslant 2\theta_t \\ \frac{\pi - 4\theta_t}{\pi} & \text{for } \theta_2 \geqslant 2\theta_t \end{pmatrix}, \tag{B5}$$

which gives the result

$$p_0 = \left(\frac{\pi - 3\theta_t}{\pi}\right)^2 = \left(1 - \frac{3}{2}p_s\right)^2. \tag{B6}$$

4. Derivation of p_0 when $\pi/4 \leqslant \theta_t \leqslant \pi/3$

In this case, the probability $p' = (\pi - 2\theta_t - |\theta_2|)/\pi$ when $\theta_t < |\theta_2| \leqslant \pi - 2\theta_t$, so that

$$p_0 = \int_{-\pi/2}^{\pi/2} \frac{d\theta_2}{\pi} \begin{pmatrix} 0 & \text{for } \theta_2 \leqslant -\pi + 2\theta_t \\ \dfrac{\pi - 2\theta_t + \theta_2}{\pi} & \text{for } -\pi + 2\theta_t \leqslant \theta_2 \leqslant -\theta_t \\ 0 & \text{for } -\theta_t \leqslant \theta_2 \leqslant \theta_t \\ \dfrac{\pi - 2\theta_t - \theta_2}{\pi} & \text{for } \theta_t \leqslant \theta_2 \leqslant \pi - 2\theta_t \\ 0 & \text{for } \theta_2 \geqslant \pi - 2\theta_t \end{pmatrix}, \tag{B7}$$

which gives the identical result as Eq. (B6). Note that $p_0 = 0$ when $\pi/3 \leqslant \theta_t \leqslant \pi/2$.

5. Derivation of p_2 when $\theta_t \leqslant \pi/3$

The function p_2 is *proportional* to the probability that the crystallographic orientation θ_2 of grain 2 lies within $[-\theta_t, \theta_t]$ (that is, within θ_t of θ_1), multiplied by the probability $|\theta_2|/\pi$ that the orientation θ_3 of grain 3 lies within $[-\theta_t, \theta_t]$ (that is, within θ_t of θ_1) *and* outside $[\theta_2 - \theta_t, \theta_2 + \theta_t]$ (that is, at least θ_t away from θ_2), integrated over all possible values of θ_2. The proportionality constant is 3, which is the number of ways of assigning the label 1 to the three grains. Expressed mathematically, this is

$$p_2 = 3\int_{-\theta_t}^{\theta_t} \frac{d\theta_2}{\pi} \begin{pmatrix} \dfrac{-\theta_2}{\pi} & \text{for } \theta_2 \leqslant 0 \\ \dfrac{\theta_2}{\pi} & \text{for } \theta_2 \geqslant 0 \end{pmatrix}, \tag{B8}$$

which gives the result

$$p_2 = 3\left(\frac{\theta_t}{\pi}\right)^2 = \frac{3}{4}p_s^2. \tag{B9}$$

6. Derivation of p_1 when $\pi/3 \leqslant \theta_t \leqslant \pi/2$

The function p_1 is *proportional* to the probability that the crystallographic orientation θ_2 of grain 2 lies within $[-\theta_t, \theta_t]$ (that is, within θ_t of θ_1), multiplied by the probability $(\pi - 2\theta_t - |\theta_2|)/\pi$ that the orientation θ_3 of grain 3 lies outside $[-\theta_t, \theta_t]$ (that is, at least θ_t away from θ_1) *and* outside $[\theta_2 - \theta_t, \theta_2 + \theta_t]$ (that is, at least θ_t away from θ_2), integrated over all possible values of θ_2. The proportionality constant is 3, which is the number of ways of assigning the label 3 to the three grains. Expressed mathematically, this is

$$p_1 = 3\int_{-\theta_t}^{\theta_t} \frac{d\theta_2}{\pi} \begin{pmatrix} \dfrac{\pi - 2\theta_t + \theta_2}{\pi} & \text{for } -\pi + 2\theta_t \leqslant \theta_2 \leqslant 0 \\ \dfrac{\pi - 2\theta_t - \theta_2}{\pi} & \text{for } 0 \leqslant \theta_2 \leqslant \pi - 2\theta_t \end{pmatrix}, \tag{B10}$$

which gives the result

$$p_1 = 3\left(1 - \frac{2\theta_t}{\pi}\right)^2 = 3(1 - p_s)^2. \tag{B11}$$

7. Derivation of p_1 when $\theta_t \leqslant \pi/3$ and p_2 when $\pi/3 \leqslant \theta_t \leqslant \pi/2$

These functions are most easily obtained from the relation $1 = p_0 + p_1 + p_2 + p_3$. Thus, in the case $\theta_t \leqslant \pi/3$,

$$p_1 = 3p_s\left(1 - \frac{5}{4}p_s\right), \tag{B12}$$

and in the case $\pi/3 \leqslant \theta_t \leqslant \pi/2$,

$$p_2 = 3(1 - p_s)(2p_s - 1). \tag{B13}$$

*Electronic address: clinton.vansiclen@inl.gov

[1] L. C. Lim and T. Watanabe, Acta Metall. Mater. **38**, 2507 (1990); G. Palumbo, P. J. King, K. T. Aust, U. Erb, and P. C. Lichtenberger, Scr. Metall. Mater. **25**, 1775 (1991); G. Palumbo, E. M. Lehockey, and P. Lin, JOM **50**, 40 (1998); T. Watanabe and S. Tsurekawa, Acta Mater. **47**, 4171 (1999); E. S. McGarrity, P. M. Duxbury, and E. A. Holm, Phys. Rev. E **71**, 026102 (2005).

[2] G. S. Was, V. Thaveeprungsriporn, and D. C. Crawford, JOM **50**, 44 (1998).

[3] V. Randle and A. Brown, Philos. Mag. A **59**, 1075 (1989); E. M. Lehockey and G. Palumbo, Mater. Sci. Eng., A **237**, 168 (1997); M. Kumar, W. E. King, and A. J. Schwartz, Acta Mater. **48**, 2081 (2000); C. A. Schuh, M. Kumar, and W. E. King, *ibid.* **51**, 687 (2003); S.-L. Lee and N. L. Richards, Mater. Sci. Eng., A **405**, 74 (2005).

[4] S. Yang, U. Krupp, H.-J. Christ, and V. B. Trindade, Adv. Eng. Mater. **7**, 723 (2005).

[5] T. Watanabe, Mater. Sci. Eng., A **176**, 39 (1994); D. Romero, L. Martinez, and L. Fionova, Acta Mater. **44**, 391 (1996); T. Watanabe and S. Tsurekawa, Mater. Sci. Eng., A **387-389**, 447 (2004).

[6] M. Frary and C. A. Schuh, Phys. Rev. B **69**, 134115 (2004).

[7] M. Frary and C. A. Schuh, Philos. Mag. **85**, 1123 (2005); Acta Mater. **53**, 4323 (2005).

[8] D. A. Van Baak, Am. J. Phys. **67**, 36 (1999).

[9] A. A. Griffith, Philos. Trans. R. Soc. London, Ser. A **221**, 163 (1920); B. R. Lawn and T. R. Wilshaw, *Fracture of Brittle Solids* (Cambridge University Press, Cambridge, UK, 1975); L. Golubovic and S. Feng, Phys. Rev. A **43**, 5223 (1991).

[10] M. D. Stephens and M. Sahimi, Phys. Rev. B **36**, 8656 (1987); P. M. Duxbury, P. L. Leath, and P. D. Beale, *ibid.* **36**, 367 (1987); B. Kahng, G. G. Batrouni, S. Redner, L. de Arcangelis, and H. J. Herrmann, *ibid.* **37**, 7625 (1988); L. de Arcangelis and H. J. Herrmann, *ibid.* **39**, 2678 (1989); A. Hansen, S. Roux, and E. L. Hinrichsen, Europhys. Lett. **13**, 517 (1990); A. Hansen, E. L. Hinrichsen, and S. Roux, Phys. Rev. B **43**, 665 (1991); S. Zapperi, A. Vespignani, and H. E. Stanley, Nature (London) **388**, 658 (1997); S. Zapperi, P. Ray, H. E. Stanley, and A. Vespignani, Phys. Rev. Lett. **78**, 1408 (1997); G. G. Batrouni and A. Hansen, *ibid.* **80**, 325 (1998); P. K. V. V. Nukala, S. Šimunović, and S. Zapperi, J. Stat. Mech.: Theory Exp. P08001 (2004); S. Pradhan, A. Hansen, and P. C. Hemmer, Phys. Rev. Lett. **95**,

125501 (2005); S. Zapperi, P. K. V. V. Nukala, and S. Šimunović, Physica A **357**, 129 (2005); S. Zapperi, P. K. V. V. Nukala, and S. Šimunović, Phys. Rev. E **71**, 026106 (2005).

[11] G. G. Batrouni and A. Hansen, Phys. Rev. Lett. **80**, 325 (1998).

[12] E. van der Giessen and V. Tvergaard, Modell. Simul. Mater. Sci. Eng. **2**, 721 (1994); P. Onck and E. van der Giessen, Comput. Mater. Sci. **13**, 90 (1998); N. Sukumar, D. J. Srolovitz, T. J. Baker, and J.-H. Prévost, Int. J. Numer. Methods Eng. **56**, 2015 (2003); V. Cannillo and W. C. Carter, J. Mater. Sci. **40**, 3993 (2005).

[13] D. Stauffer and A. Aharony, *Introduction to Percolation Theory*, 2nd. ed. (Taylor & Francis, London, 1994).

[14] X. Tingdong and Z. Lei, Philos. Mag. Lett. **84**, 225 (2004).

[15] J. H. Meinke, E. S. McGarrity, P. M. Duxbury, and E. A. Holm, Phys. Rev. E **68**, 066107 (2003).

[16] E. S. McGarrity, P. M. Duxbury, and E. A. Holm, Phys. Rev. E **71**, 026102 (2005).

[17] A. Pyzalla, B. Camin, T. Buslaps, M. Di Michiel, H. Kaminski, A. Kottar, A. Pernack, and W. Reimers, Science **308**, 92 (2005).